GeoHealth

Supporting Information for

Investigating the Impact of Irrigation on Malaria Larval Habitats and Transmission Using a Hydrology-based Model

Ai-Ling Jiang[1], Ming-Chieh Lee[2], Prashanth Selvaraj[3], Teshome Degefa[4, 5], Hallelujah Getachew[4,5,6], Hailu Merga[7], Delenasaw Yewhalaw[4,5], Guiyun Yan[2], Kuolin Hsu[1]

[1] Center for Hydrometeorology and Remote Sensing, Department of Civil and Environmental Engineering, University of California Irvine, Irvine, CA, USA

[2] Department of Population Health and Disease Prevention, School of Public Health, Susan and Henry Samueli College of Health Sciences, University of California Irvine, Irvine, CA, USA

[3] Institute for Disease Modeling, Bill and Melinda Gates Foundation, Seattle, WA, USA

[4] School of Medical Laboratory Sciences, Institute of Health, Jimma University, Jimma, Ethiopia

[5] Tropical and Infectious Diseases Research Center (TIDRC), Jimma University, Jimma, Ethiopia

[6] Department of Medical Laboratory Technology, Arbaminch College of Health Sciences, Arba Minch, Ethiopia

[7] Department of Epidemiology, Institute of Health, Jimma University, Jimma, Ethiopia

Contents of this file

Introduction

This file contains additional information on data collection, model development, calibration and simulation results.

Text S1. Larval density estimation

In the study area, the surveyed larval habitats include drainage ditch, river edge/reservoir shoreline, swamp/marsh, rice puddle, animal footprint, tire track/road puddle, man-made pond, natural pond/rain pool, rock pool, water container, irrigation canal, and brick pit. The larval habitats were classified as temporary, semi-permanent, or permanent based on their natural characteristics. Since larval density can be significantly different in the dry and rainy seasons (Hinne et al., 2021; Kweka et al., 2012) and the timing and duration of the survey periods were inconsistent, we sorted the measured larval densities from the 769 sample points (Figure 1) into the dry season (January to April; November to December) and the rainy season (May to October). We then calculated the average larval density for each season as shown in Figure S4.

In the surveyed area, the larval density for temporary habitats was higher in the rainy season than in the dry season during which the habitats are less stable. On the other hand, the larval densities for semi-permanent and permanent habitats were higher in the dry season. Most of the semi-permanent and permanent habitats were associated with river edges and swamps, whereby the larvae are prone to flushing in the rainy season. Finally, the larval density in Table 1 was calculated based on the average dry season and rainy season densities.

Text S2. Irrigation schedule design

Figure S6 shows the monthly irrigation schedule obtained from the Arjo-Didessa Sugar Factory, which is tailored to the sugarcane planting cycle.

To model irrigation in ParFlow-CLM, the irrigation interval and rate are required user inputs. A report provided by the factory recommended 8-12 days for the design of the local irrigation system, so we set the irrigation interval as 10 days.

To determine the irrigation rate, we first calculated the irrigation depth, defined as the amount of water that needs to be applied when the soil water content is depleted to the wilting point. The irrigation depth ($IrrD$) was calculated as

$$IrrD = (FC - WP) \times Depth_{soil}, \tag{S1}$$

where FC is the field capacity, WP is the permanent wilting point and $Depth_{soil}$ is the soil depth.

The study area is characterized by clay and clay loam with low permeability. Based on resources by the Northeast Region Certified Crop Advisor (https://nrcca.cals.cornell.edu/soil/CA2/CA0212.1-3.php), the field capacity volumetric soil moisture content of clay was set as 50%, and the wilting point volumetric soil moisture content was set as 15%. A soil depth of 2 m was assumed. Using Equation (S1), an irrigation depth of 700 mm was obtained.

We configured the irrigation to be applied when 50% of the irrigation depth was depleted; hence, the actual irrigation depth to be applied over the 10-day irrigation interval was 350 mm. Adopting an intermittent irrigation strategy, we set the irrigation to be applied for 22 hours a day over 3 days within the 10-day cycle. The irrigation rate was then calculated to be 5.3 mm/hour.

Text S3. Model calibration

At each grid cell, ponding is assumed to occur if the soil saturation exceeds the threshold, θ. Therefore, the threshold was calibrated to ensure that the model will predict the occurrence of ponding at locations in line with the field-surveyed larval habitats for soil saturation above θ. The value for θ was obtained based on a sensitivity analysis by altering the threshold and noting the corresponding change in the probability of detection (POD). The POD determines if the model can predict an aquatic habitat successfully and can be calculated based on the ratio of the number of successful predictions or hits, H, to the total number of samples, S:

$$POD = H/S, \tag{S2}$$

Figure S8 shows the results of the sensitivity analysis. Generally, the POD curve is higher for the simulation excluding dry season. This is because irrigation was only approximated by a simplified scheme in the dry season and may not reflect the localized irrigation dynamics. As the threshold was lowered, POD increased because ponding occurred across a larger area in the model. The influence of topography on the ponding was weakened, and the soil type became the dominant factor. On the other hand, when the threshold was increased, less ponding was predicted, resulting in a lower POD but the topographic variability was better represented. Therefore, we selected a threshold of 0.75 for a reasonable POD of 0.66 (excluding dry season) without obscuring topographic variability.

In EMOD, we calibrated 15 key parameters identified from a preliminary sensitivity analysis, and Table S3 presents the calibrated values. Using the calibrated parameters, we compared the simulated prevalence rate against field data for January 2018 and October 2018 (Figure S9). The results are within the same order of magnitude. In addition, we compared the simulated monthly number of clinical cases with the recorded malaria cases from April 2018 to May 2020 (Figure S10). Apart from the two peaks missed in October 2018 and November 2019, the simulated malaria cases compare reasonably well with observation in terms of magnitude and pattern. As the clinical malaria cases were sourced from major hospitals within the study area, the two peaks in recorded cases could be anomalous due to an influx of patients from outside seeking treatment at the hospitals. Overall, the model shows a good agreement with the field observation.

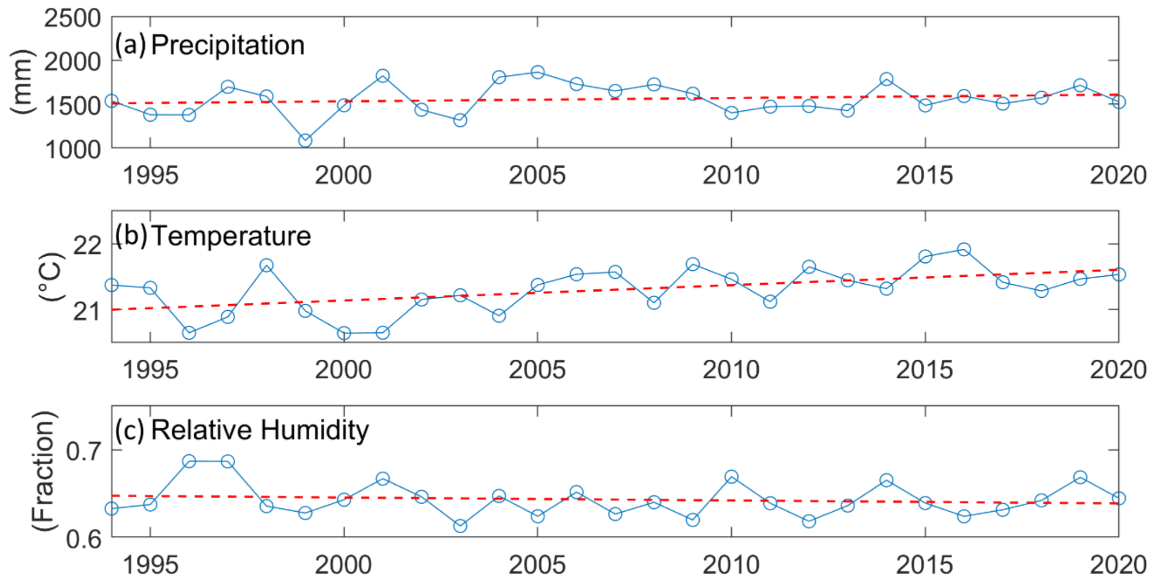

Figure S1. Annual climate data from PERSIANN-CCS-CDR and ERA5 for the study area. (a) total precipitation, (b) average temperature and (c) average relative humidity. The red dashed line represents the linear trendline in each subplot.

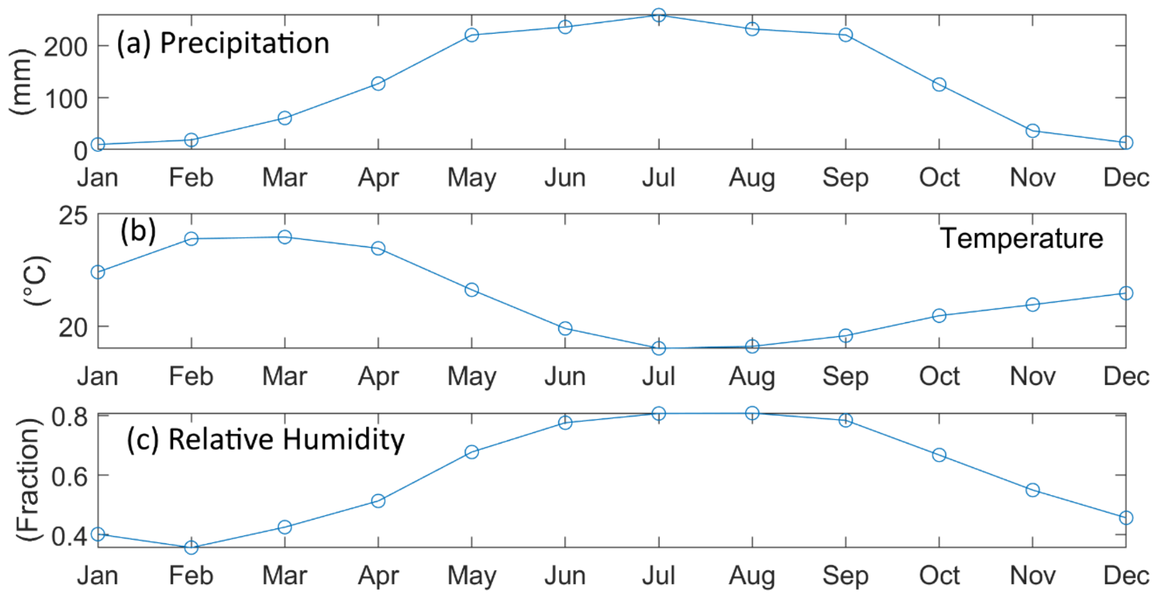

Figure S2. Monthly climate data (averaged from 1994 to 2020) derived from PERSIANN-CCS-CDR and ERA5 climate data for the study area. (a) total precipitation, (b) average temperature, and (c) average relative humidity.

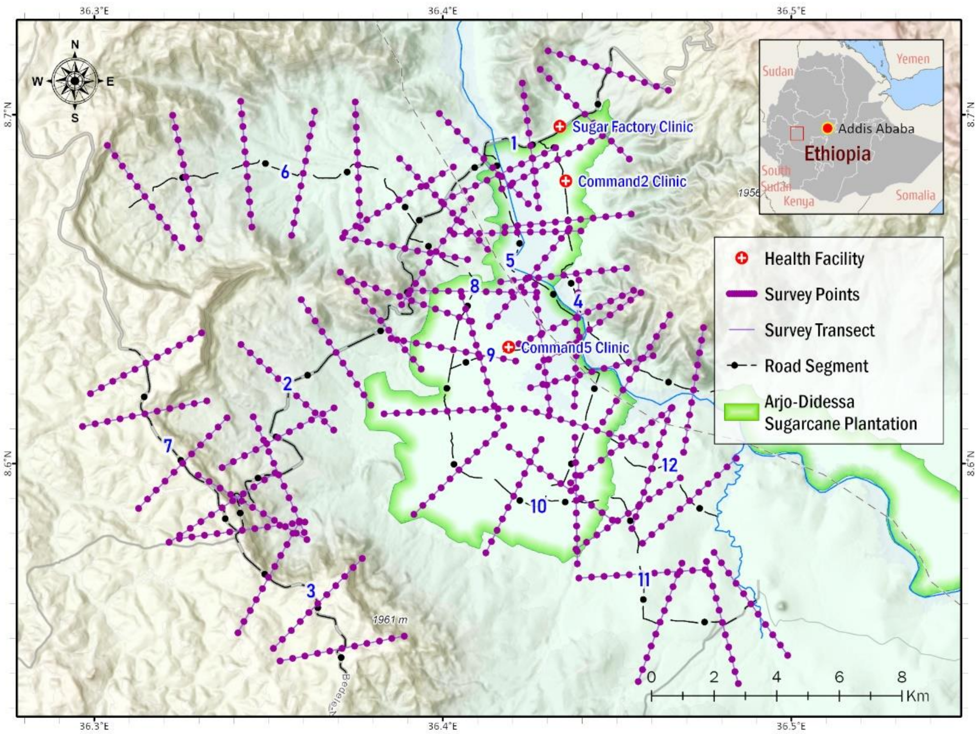

Figure S3. Land use survey locations.

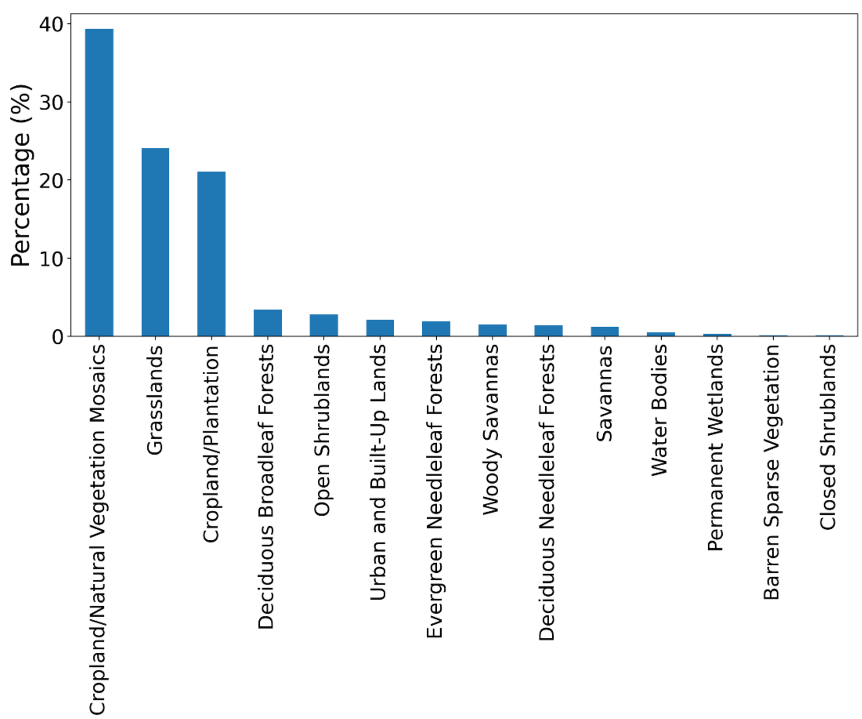

Figure S4. Percentage distribution of International Geosphere-Biosphere Programme type from land use survey.

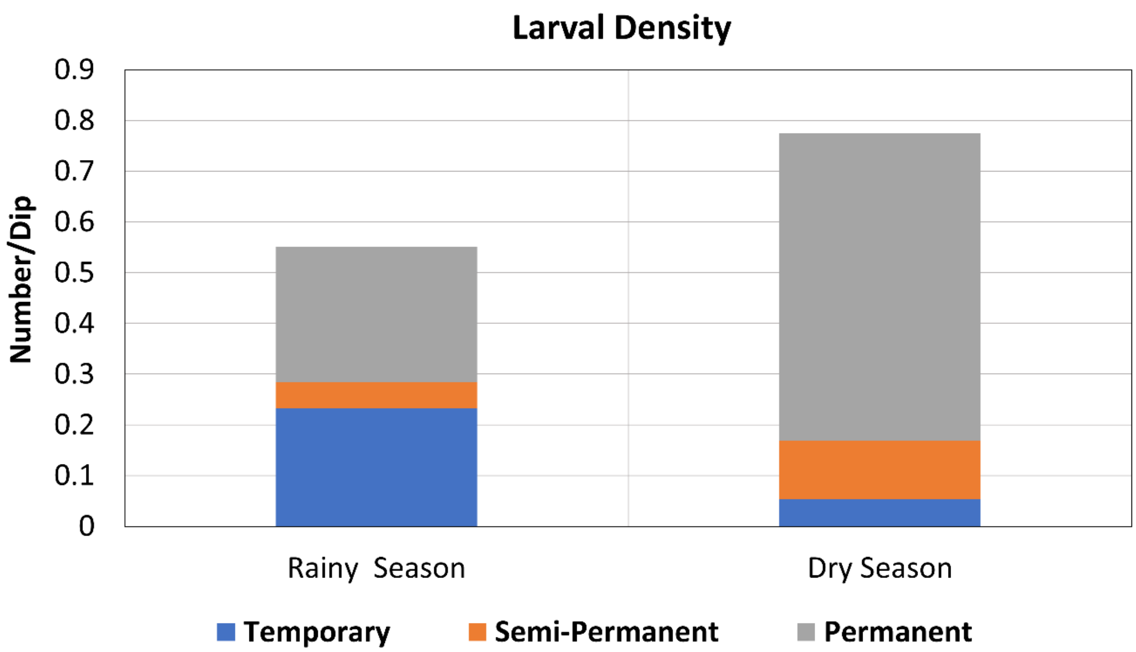

Figure S5. Average larval densities for temporary, semi-permanent, and permanent habitats during rainy and dry seasons from field survey.

(a)	1st Year (Virgin Planting)												2nd Year (Virgin Planting)												1st Ratoon			
Mn	1	2	3	4	5	6	7	8	9	10	11	12	1	2	3	4	5	6	7	8	9	10	11	12	1	2	3	4
Sym.	MA	H	H	LW	P	P	P	P	RF	RF	IR	IR	IR	IR	IR	IR	RF	RF	RF	RF	RF	RF	MA	MA	MA	H	IR	IR

(b)	1st Ratoon												2nd Ratoon												Virgin Planting			
Mn	1	2	3	4	5	6	7	8	9	10	11	12	1	2	3	4	5	6	7	8	9	10	11	12	1	2	3	4
Sym.	MA	H	IR	IR	RF	RF	RF	RF	RF	RF	MA	MA	MA	H	IR	IR	RF	RF	RF	RF	RF	RF	MA	MA	MA	H	H	LW

Figure S6. Arjo-Didessa Sugar Factory sugarcane plantation irrigation schedule. A typical sugar planting schedule includes (a) a 2-year cycle for virgin planting and (b) a 1-year cycle for the following 2 ratoons. MA: Maturity/water drain; H: Harvesting; LW: Land work; P: Planting; RF: Rainfed; IR: Irrigation.

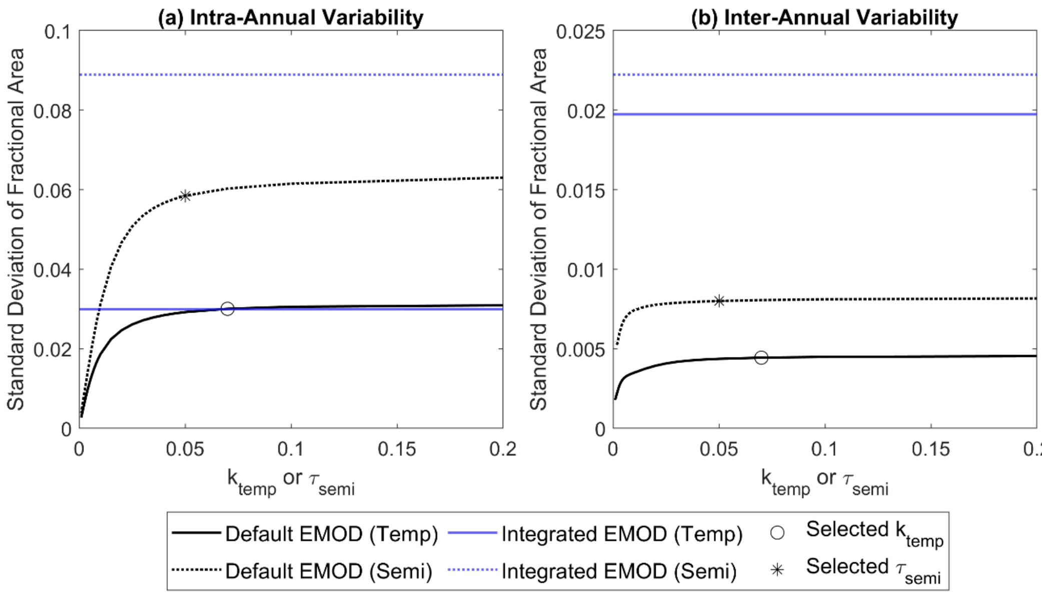

Figure S7. Adjustment of decay factors for temporary and semi-permanent habitats in default EMOD function. The objective was to match the (a) intra-annual variability and (b) inter-annual variability of the habitats from the hydrologic model as closely as possible. The decay factor of semi-permanent habitat also had to be smaller than that of temporary habitat. Intra-annual variability was measured in terms of the standard deviation of the 20-year average habitat area for each day of the year. Inter-annual variability was characterized by the standard deviation of the annual average habitat area for each year.

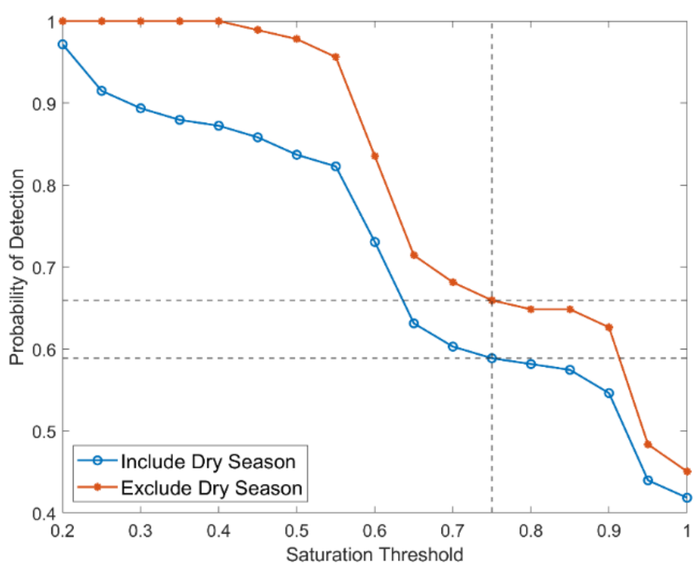

Figure S8. Sensitivity analysis of the probability of detection to saturation threshold. The probability of detection determines if the model can predict an aquatic habitat successfully and can be calculated based on the ratio of successful predictions to the total number of observations. The dotted vertical line corresponds to the selected threshold of 0.75, which results in a reasonable POD of 0.66 excluding dry season and a POD of 0.59 including dry season.

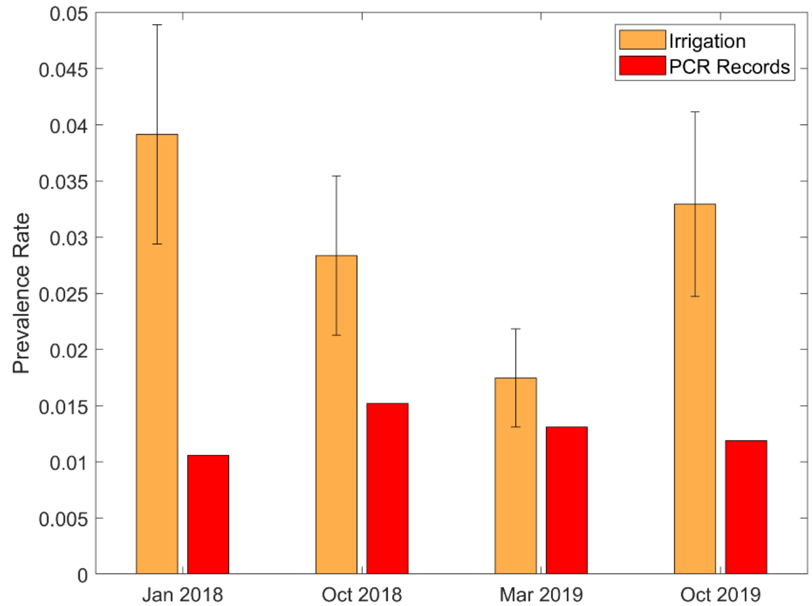

Figure S9. Comparison of simulated monthly average prevalence rate in *Irrigation* and measured prevalence diagnosed by Polymerase Chain Reaction (PCR). The whisker on the bar plot represents one standard error.

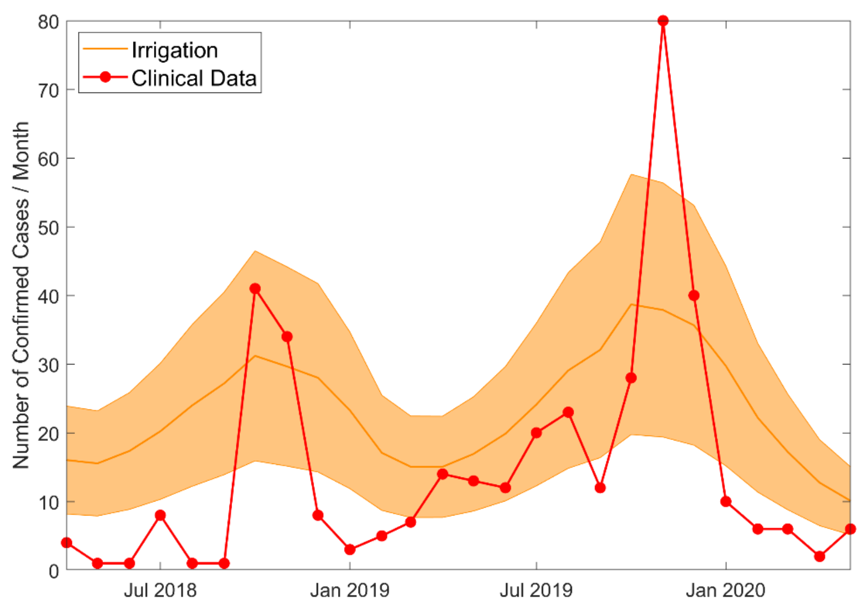

Figure S10. Comparison of simulated monthly confirmed cases in *Irrigation* and clinical data. The orange band indicates the 95% confidence interval.

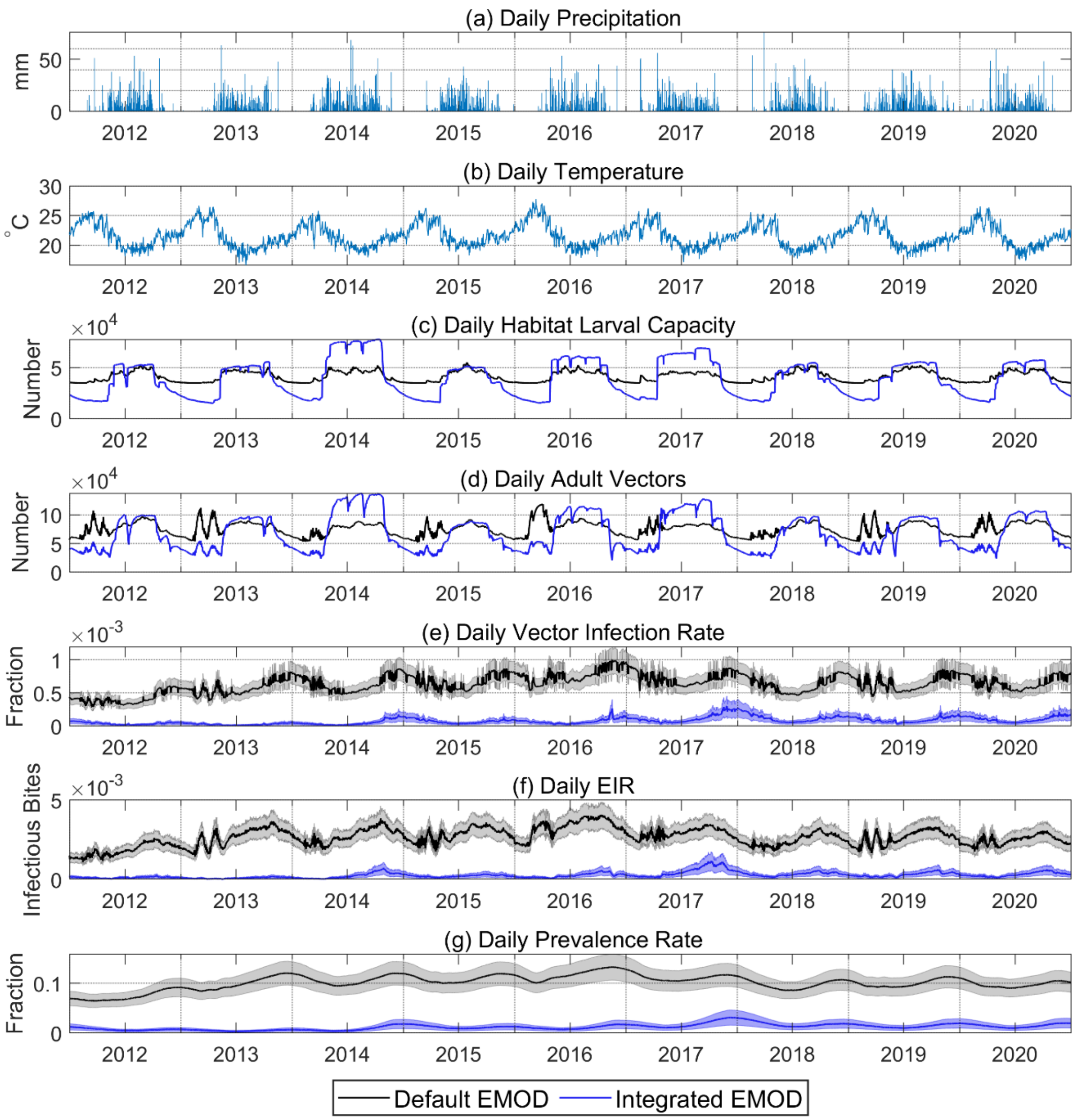

Figure S11. Time series of daily climate data and comparison of simulated daily malaria transmission results between *Default EMOD* and *Integrated EMOD*. Climate data include (a) precipitation and (b) temperature. Malaria transmission results include (c) habitat larval capacity, (d) adult vector abundance, (e) adult vector infection rate, (f) entomological inoculation rate and (g) parasite prevalence rate. The simulation was performed for 20 years from 2000 to 2020, but here we only show the results from 2010 to 2020 for simplicity.

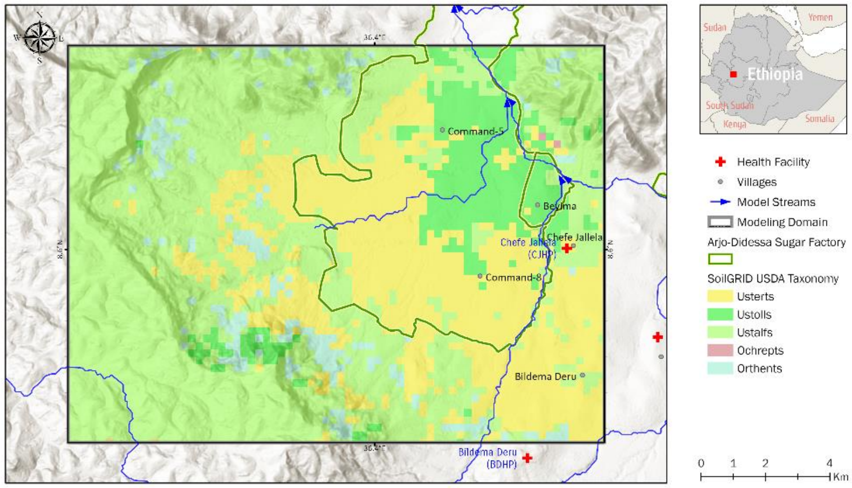

Figure S12. The distribution of the top two-meter soil types in USDA soil taxonomy from SoilGrids250m TAXOUSDA dataset. Most soil types in this area are characterized as clay or clay loam with low permeability ranging from 0.0015 to 0.015 m/h.

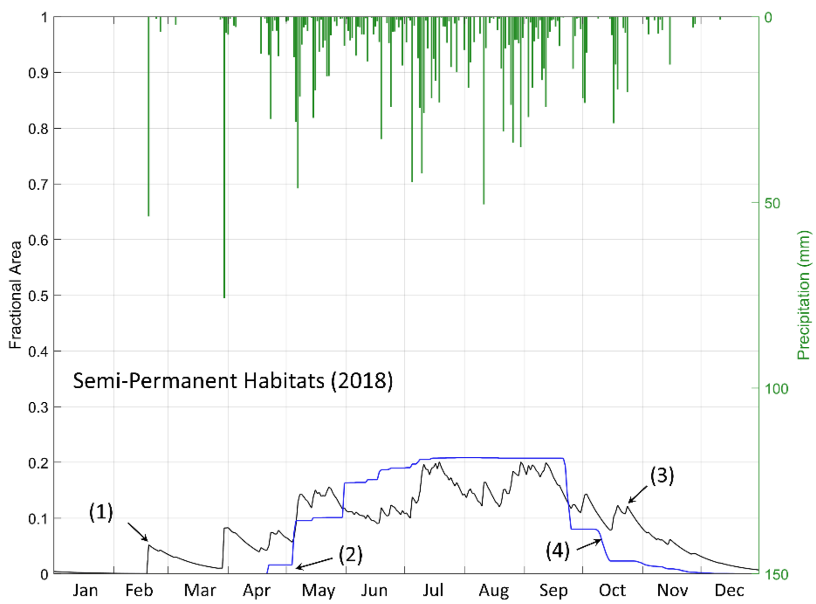

Figure S13. Comparison of simulated semi-permanent habitats between *Default EMOD* (black line) and *Integrated EMOD* (blue line) in 2018. Earlier rising limb in *Default EMOD*: (1) no infiltration, new ponds created instantaneously by rainfall; (2) ponds formed sometime after rainfall when soil saturation exceeded the threshold. Delayed falling limb in *Default EMOD*: (3) habitat area continued to increase with rainfall; (4) pond drained/dried up and soil became unsaturated after a period without rainfall, new rainfall insufficient to create ponding as soil saturation remained below threshold.

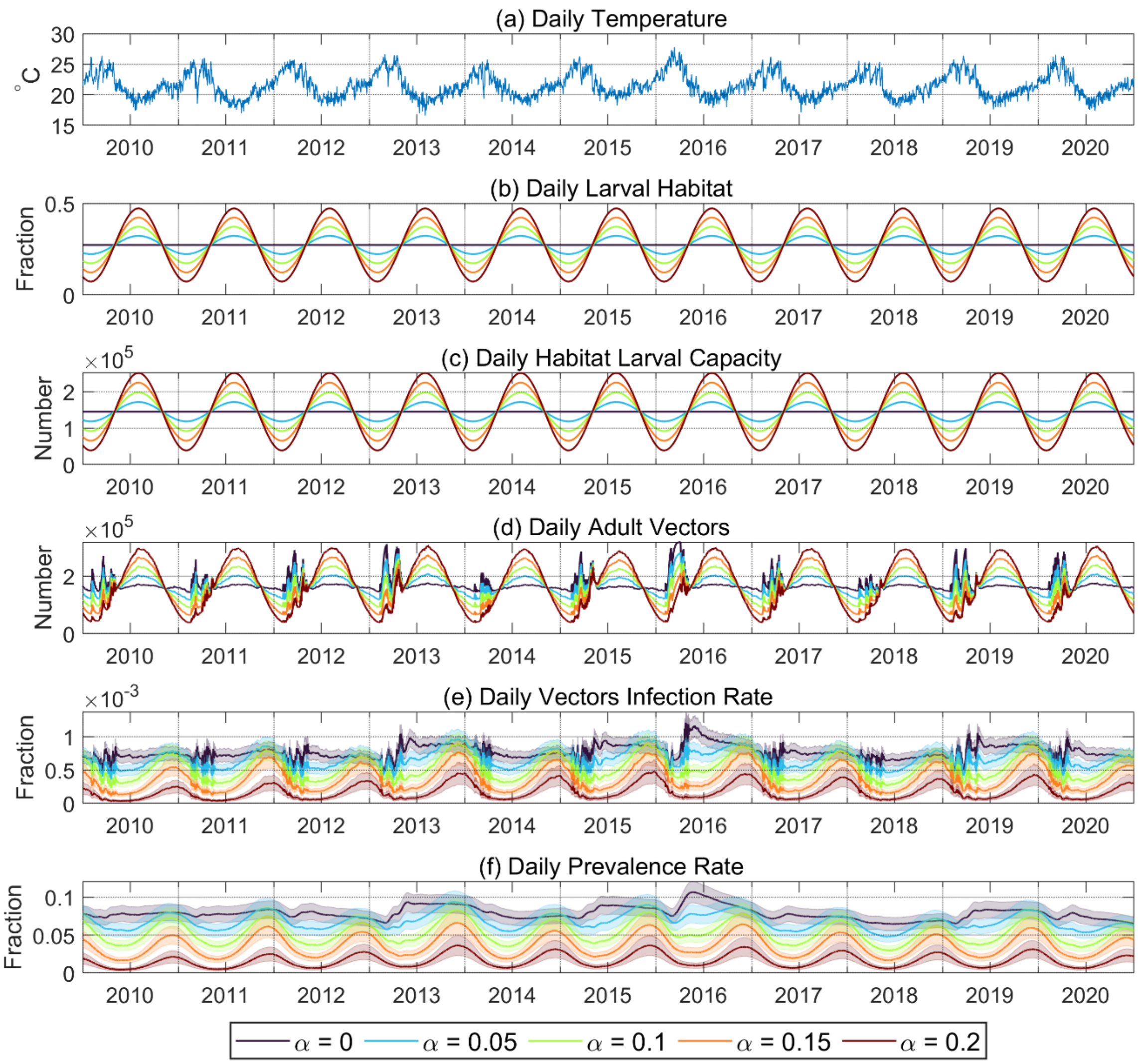

Figure S14. Simulation results from sensitivity analysis of malaria transmission to different amplitudes of larval habitat seasonality, $\boldsymbol{\alpha}$. Time series include (a) daily temperature, (b) synthetic sinusoidal larval habitat, (c) habitat larval capacity, (d) adult vector abundance, (e) adult vector infection rate and (f) parasite prevalence rate.

Table S1. Input data for ParFlow-CLM and EMOD.

Variable	Resolution	Latency	Source
Topography	5-meter	-	ALOS WORLD 3D Topographic Data (Takaku et al., 2016; Takaku and Tadono, 2017)
Precipitation	0.04°×0.04°, 3-hourly	~1 hour	Precipitation Estimation from Remotely Sensed Information using Artificial Neural Networks -Cloud Classification System- Climate Data Record (PERSIANN-CCS-CDR) (Sadeghi et al., 2021)
Surface Solar Radiation Downwards	0.25°×0.25°, 1-hourly	5 days	The Fifth Generation European Centre for Medium-Range Weather Forecasts Reanalysis (ERA5) (Hersbach et al., 2020, 2018)
Surface Thermal Radiation Downwards	0.25°×0.25°, 1-hourly	5 days	ERA5
Air Temperature (2m above ground surface)	0.25°×0.25°, 1-hourly	5 days	ERA5
Skin Temperature	0.25°×0.25°, 1-hourly	5 days	ERA5
Surface Pressure	0.25°×0.25°, 1-hourly	5 days	ERA5
Water-vapor specific humidity	0.25°×0.25°, 1-hourly	5 days	ERA5
North-to-South Component of Wind Speed (10m above ground surface)	0.25°×0.25°, 1-hourly	5 days	ERA5
East-to-West Component of Wind Speed (10m above ground surface)	0.25°×0.25°, 1-hourly	5 days	ERA5
Land Use (2000)	30-meter	-	Global Land Cover Mapping Project (GlobeLand30) (Chen et al., 2015)
Land Use (2010)	30-meter	-	GlobeLand30
Land Use (2020)	30-meter	-	GlobeLand30

Soil Type	250-meter	-	SoilGrids250m, TAXOUSDA (Hengl et al., 2017)
Depth to Bedrock	250-meter	-	SoilGrids250m, BDRICM (Hengl et al., 2017)
Near Surface Permeability (< 100 m)	Regional Scale	-	GLobal HYdrogeology MaPS 2.0 (GLHYMPS, 2.0) (Gleeson et al., 2014)

Table S2. Field data for ParFlow-CLM and EMOD validation.

Variable	Period	Number of Samples	Source
Land Use	July 2021	578	Site survey
Larval Habitat	2017-2021	769	Site survey
Population	2018-2021	-	Site survey
Prevalence Rate	January, October 2018; March, October 2019	4	Site survey
Clinical Case	April 2018-May 2020	26	Site survey

Table S3. Calibrated parameters in EMOD.

Parameter	Value
Antibody Memory Level	0.298
Base Sporozoite Survival Fraction	0.1667
Cytokine Gametocyte Inactivation	0.01335
Falciparum PfEMP1 Variants	150
Mean Sporozoites Per Bite	6
Merozoites Per Hepatocyte	990
Min Adapted Response	0.0174
Pyrogenic Threshold	500
Adult Life Expectancy	20
Male Life Expectancy	14
Aquatic Arrhenius 1	85,884,000,000

Aquatic Arrhenius 2	7,495
Infected Arrhenius 1	119,340,000,000
Infected Arrhenius 2	7,502
Scaling factor for larval capacity	1.66×10^{-5}

Table S4. Spatial average of adult vector and parasite prevalence rate from the dry season (November 2016 to April 2017) and the rainy season (May 2017 to October 2017).

Scenario	Dry Season		Rainy Season	
	Adult Vectors (# /km^2)	Prevalence (Fraction)	Adult Vectors (# /km^2)	Prevalence (Fraction)
Default EMOD	697	0.120	800	0.108
Integrated EMOD (Non-Irrigation)	451	0.111	961	0.107
Irrigation	889	0.154	1,140	0.182

References

Chen, Jun, Chen, Jin, Liao, A., Cao, X., Chen, L., Chen, X., He, C., Han, G., Peng, S., Lu, M., Zhang, W., Tong, X., Mills, J., 2015. Global land cover mapping at 30 m resolution: A POK-based operational approach. ISPRS J. Photogramm. Remote Sens. 103, 7–27. https://doi.org/10.1016/j.isprsjprs.2014.09.002

Gleeson, T., Moosdorf, N., Hartmann, J., van Beek, L.P.H., 2014. A glimpse beneath earth's surface: GLobal HYdrogeology MaPS (GLHYMPS) of permeability and porosity. Geophys. Res. Lett. 41, 3891–3898. https://doi.org/10.1002/2014GL059856

Hengl, T., Mendes de Jesus, J., Heuvelink, G.B.M., Ruiperez Gonzalez, M., Kilibarda, M., Blagotić, A., Shangguan, W., Wright, M.N., Geng, X., Bauer-Marschallinger, B., Guevara, M.A., Vargas, R., MacMillan, R.A., Batjes, N.H., Leenaars, J.G.B., Ribeiro, E., Wheeler, I., Mantel, S., Kempen, B., 2017. SoilGrids250m: Global gridded soil information based on machine learning. PLoS One 12, e0169748. https://doi.org/10.1371/journal.pone.0169748

Hersbach, H., Bell, B., Berrisford, P., Biavati, G., Horányi, A., Muñoz Sabater, J., Nicolas, J., Peubey, C., Radu, R., Rozum, I., Schepers, D., Simmons, A., Soci, C., Dee, D., Thépaut, J.-N., 2018. ERA5 hourly data on single levels from 1959 to present [WWW Document]. Copernicus Clim. Chang. Serv. Clim. Data Store. https://doi.org/10.24381/cds.adbb2d47

Hersbach, H., Bell, B., Berrisford, P., Hirahara, S., Horányi, A., Muñoz-Sabater, J., Nicolas, J., Peubey, C., Radu, R., Schepers, D., Simmons, A., Soci, C., Abdalla, S., Abellan, X., Balsamo, G., Bechtold, P., Biavati, G., Bidlot, J., Bonavita, M., De Chiara, G., Dahlgren, P., Dee, D., Diamantakis, M., Dragani, R., Flemming, J., Forbes, R., Fuentes, M., Geer, A., Haimberger, L., Healy, S., Hogan, R.J., Hólm, E., Janisková, M., Keeley, S., Laloyaux, P., Lopez, P., Lupu, C., Radnoti, G., de Rosnay, P., Rozum, I., Vamborg, F., Villaume, S., Thépaut, J.N., 2020. The ERA5 global reanalysis. Q. J. R. Meteorol. Soc. 146, 1999–2049. https://doi.org/10.1002/qj.3803

Hinne, I.A., Attah, S.K., Mensah, B.A., Forson, A.O., Afrane, Y.A., 2021. Larval habitat diversity and Anopheles mosquito species distribution in different ecological zones in Ghana. Parasites and Vectors 14, 1–14. https://doi.org/10.1186/s13071-021-04701-w

Kweka, E.J., Zhou, G., Munga, S., Lee, M.C., Atieli, H.E., Nyindo, M., Githeko, A.K., Yan, G., 2012. Anopheline Larval Habitats Seasonality and Species Distribution: A Prerequisite for Effective Targeted Larval Habitats Control Programmes. PLoS One 7, e52084. https://doi.org/10.1371/journal.pone.0052084

Sadeghi, M., Nguyen, P., Naeini, M.R., Hsu, K., Braithwaite, D., Sorooshian, S., 2021. PERSIANN-CCS-CDR, a 3-hourly 0.04° global precipitation climate data record for heavy precipitation studies. Sci. Data 8, 1–11. https://doi.org/10.1038/s41597-021-00940-9

Takaku, J., Tadono, T., 2017. Quality updates of 'AW3D' global DSM generated from ALOS PRISM, in: 2017 IEEE International Geoscience and Remote Sensing Symposium (IGARSS). IEEE, pp. 5666–5669. https://doi.org/10.1109/IGARSS.2017.8128293

Takaku, J., Tadono, T., Tsutsui, K., Ichikawa, M., 2016. Validation of 'AW3D' Global DSM Generated from ALOS PRISM. ISPRS Ann. Photogramm. Remote Sens. Spat. Inf. Sci. III–4, 25–31. https://doi.org/10.5194/isprsannals-III-4-25-2016